Carbon 130 (2018) 11–18

Contents lists available at ScienceDirect

Carbon

journal homepage: www.elsevier.com/locate/carbon

Electrochemical intercalation of fullerene and hydrofullerene with sodium

S. Scaravonati [a], G. Magnani [a], M. Gaboardi [a, b], G. Allodi [a], M. Riccò [a], D. Pontiroli [a, *]

[a] Dipartimento di Scienze Matematiche, Fisiche e Informatiche, Università degli Studi di Parma, Parco Area delle Scienze, 7/a, 43124 Parma, Italy
[b] ISIS Facility, Rutherford Appleton Laboratory, Chilton, Didcot, Oxfordshire OX11 0QX, United Kingdom

ARTICLE INFO

Article history:
Received 5 September 2017
Received in revised form
20 December 2017
Accepted 24 December 2017
Available online 27 December 2017

ABSTRACT

We herein report on the ability of fullerene C_{60} and hydrogenated fullerene $C_{60}H_x$ (x~39) to operate as negative electrodes in novel Na-ion batteries. Building upon the known solubility of C_{60} in common organic electrolytes used in batteries, we developed a suitably optimized solid-state Na-(polyethylene oxide) electrolyte for this application. Electrochemical and structural properties of the fullerene electrodes were investigated through cyclic voltammetry, fixed-current charge/discharge of the electrodes, impedance spectroscopy and powder X-ray diffraction. Both C_{60} and hydrogenated C_{60} have been electrochemically intercalated with sodium. Specific capacities after the first cycle are 250 mAh g^{-1} and 230 mAh g^{-1} for C_{60} and $C_{60}H_x$ respectively. However, C_{60} electrode shows a strong irreversible character after the first discharge, probably due to the formation of stable polymeric Na_xC_{60} phases, where Na^+ ions diffusion is hindered. On the contrary, $C_{60}H_x$ displays better reversibility, suggesting that hydrogenation of the buckyball could be effective to preserve sufficiently large interstitial pathways for Na^+ diffusion upon intercalation.

1. Introduction

Li-ion batteries (LIBs) are currently the most widespread rechargeable power sources employed in various portable devices [1], but one of their main drawbacks is represented by the relative scarcity of lithium in the Earth's crust, preventing their large scale implementation, especially in the automotive field [2]. The replacement of lithium with sodium offers an alternative strategy, since sodium is largely available in nature [3]. The chemical similarity shared by the two alkali metals allows a partial recover of the Li-ion battery technology for Na-ion batteries (SIBs); in fact, as far as cathode materials are concerned, several layered transition metal oxides and fluorophosphates were already identified as suitable for commercial use [4,5]. However, typical anode insertion materials for LIBs, such as silicon and graphite, do not work in SIBs [3].

In particular, Na^+ does not intercalate easily in graphite for sterical reasons [6] and only stage-2 samples can be obtained, corresponding to a stoichiometry of NaC_{64}, which is unsuitable for applications [7]. By co-intercalating Na^+ into graphite with appropriate solvents, a reversible capacity of 150 mAh/g with high cycle stability was obtained in graphite negative electrodes operating with ether-based electrolytes, even if the intercalation is accompanied by a strong volume expansion [8]. Better performances can be reached by expanding graphite through oxidation, which can increase specific capacity up to 284 mAh/g, although with low efficiency [9]. The successful intercalation of sodium can be also obtained whenever the stacking order is lost, such as in hard-carbon materials. Hard-carbon and anthracite-derived electrodes proved to be potentially interesting as SIBs anodes, showing capacities of 355 mAh/g and 222 mAh/g respectively, which can be further increased by doping with nitrogen or boron [10]. Hard carbon electrodes are currently the most widely used carbon-based anode materials for SIBs, thanks to their low sodium intercalation potential below 0.1 V, even if they still suffer from high reversibility loss [11]. Several electrolytes and additives have been proposed to limit the irreversibility problems in carbon, by improving the formation of the solid electrolyte interphase (SEI) [12–14].

On the other hand, use of carbon nanomaterials as negative electrodes in SIBs, such as carbon nanotubes, carbon nanofibers and graphene related materials, proved to be effective to improve performances, in particular the rate capability in devices [15–19]. Recently, we found 248 mAh/g reversible capacity after 50 cycles in

* Corresponding author.
E-mail address: daniele.pontiroli@fis.unipr.it (D. Pontiroli).

https://doi.org/10.1016/j.carbon.2017.12.107
0008-6223/

thermally exfoliated graphite oxide (TEGO), 491 mAh/g after 20 cycles in hydrogen-treated TEGO and up to 826 mAh/g reversible capacity after 25 cycles for Nickel nanoparticles decorated TEGO [20]. Such electrodes also displayed good rate capability, although Na^+ insertion was found to be largely irreversible and also related to pseudocapacitive processes [21,22].

In this complex scenario, a possible alternative among carbonaceous anode materials for SIBs can be represented by fullerene-based compounds. Efficient macroscopic production of Buckminsterfullerene C_{60}, the best representative of this class of compounds, has been known since 1990, through the use of the Krätschmer and Huffman method, which is scalable at the industrial level, making available in principle large quantities of C_{60} for practical applications [23]. Alkali intercalation in fullerenes is another well-known process, which is accomplished by the progressive filling of the triple-degenerated narrow C_{60} LUMO band [24]. This can eventually bring to the onset of unconventional structural and electronic phenomena in fullerides, such as C_{60} polymerization [25,26], metal-to-insulator transitions [27] and even high-temperature superconductivity [28,29]. The redox properties of fullerenes received noticeable attention in the past, for their possible use as negative electrodes in LIBs [30–32] and up to six stable electrochemical states of C_{60} were found by means of cyclic voltammetry by operating with suitable solvents, such as acetonitrile and toluene, which proved the ability of the molecule to reversibly accept up to 6 electrons upon reduction (respectively -0.98, -1.37, -1.87, -2.35, -2.85 and -3.26 V vs Fc/Fc^+) [33].

A significant problem of fullerene films is however the increased solubility of fullerene anions in conventional solvents used as electrolytes, which would lead to the dissolution of the anode upon doping. In particular, $C60^{n-}$ turn out to be soluble in ethylene carbonate/dimethyl carbonate (EC/DMC) mixture commonly used in liquid electrolytes for LIBs and SIBs, while it shows low solubility in polyethylene glycol dimethyl ether (PEGDME) [34]. To overcome this problem, fullerene derivative polymers were proposed [35], as well as the use of solid polymer electrolytes instead of liquid ones [31,34].

Early studies on solid-state cells demonstrated the feasibility to electrochemically intercalate fullerene electrodes with both lithium and sodium. In particular, in the case of lithium doping, Chabre et al. [31] managed to insert up to 12 Li^+ ions per C_{60} operating with polyethylene oxide (PEO)-$LiClO_4$ electrolyte and pure C_{60} films, while Loutfy et al. highlighted exceptional capacities exceeding 1000 mAh/g in half-cells operating with hydrogenated C_{60} and C_{70} based anodes [34]. In the case of sodium doping, to our knowledge, very few works are indeed present in literature. Lemont et al. reported the intercalation of up to 6 Na^+ per C_{60} molecule using PEO based electrolytes, but the results are not clear, because strongly influenced by extrinsic conditions [31,36]. On the other hand, physical doping of fullerenes with sodium is a well-documented phenomenon [37] and, thanks to the formation of Na heteroclusters into the larger interstitial voids of the *fcc* C_{60} lattice, even the stoichiometry of $Na_{11}C_{60}$ can be reached [38]. Incidentally, this class of alkali cluster intercalated fullerides (with Li and Na) recently proved to be also highly efficient reversible direct and indirect solid-state hydrogen absorbers [39–42].

A renewed interest of the use of fullerene C_{60} as active material in novel ionic batteries arose from the evidence of room-temperature superionic conductivity in the Li^+ intercalated fullerene polymer Li_4C_{60} [43], which seems to be supported by the presence of sufficiently large three-dimensional pathways among C_{60} units, by the presence of intrinsic unoccupied Li^+ interstitial sites and by the coupling of the low-frequency optic modes of the Li^+ ions to the soft structure of the polymer [44]. Ion inter-site diffusion was observed also in Li_xC_{60} compounds at higher doping-level (where C_{60} polymerization is lost and Li^+ ions were found to clusterize in the octahedral voids of the *fcc* lattice), by means of Solid State NMR and impedance spectroscopy [45,46], and even in mixed Li-Na intercalated C_{60} phases [47]. However, in Li fullerides it was found that a sizeable electronic conductivity generally competes with ion diffusion, thus making these systems unsuitable for a direct use as solid-state electrolytes in Li-ion batteries [48–50]. It is worth noting that polymerized C_{60} lattice is also able to sustain sizeable Mg^{2+} ion diffusion at room temperature [51], thanks to the unique ability of fullerene to delocalize its charge on the entire cage, and recently secondary Mg-ion batteries with good rate performances were produced exploiting C_{60} as a cathode material [52].

In this manuscript, we investigate the ability of fullerene C_{60} and highly hydrogenated fullerene $C_{60}H_x$ (x~39) to operate as negative electrodes of novel all-solid-state Na-ion batteries. After the optimization of a suitable solid-state electrolyte, which was chosen due to the solubility of C_{60} in liquid electrolyte solvents, the electrochemical activity of C_{60} and $C_{60}H_x$ electrodes was probed with cyclic voltammetry, galvanostatic charge/discharge measurements, impedance spectroscopy and powder X-ray diffraction.

2. Materials and methods

C_{60} electrodes were prepared starting from commercial fullerene C_{60} (MER Corporation, 99+% purity) and $C_{60}H_x$ (MER Corporation, 99+% purity) powders. Here, $C_{60}H_x$ is a mixture of hydrogenated fullerenes with an average value of x~39. The active materials (85 wt%) were mixed with polyvinylidene fluoride binder (PVDF, Solef® 6010 and 6020 respectively for C_{60} and $C_{60}H_x$, Solvay, 10 wt%) and carbon-black (Super C65, Timcal, 5 wt%). Few drops of N-methyl-pyrrolidone (NMP, Sigma Aldrich anhydrous, 99.5% purity) were added and the resulted slurry was stirred for 12 h. Reagents were used as received, except for C_{60}, which was vacuum dried at 250 °C for 12 h beforehand, in order to remove possible traces of solvents. The electrodes were obtained by spreading the slurry on 100 μm thick aluminum foil or, alternatively, 300 μm thick copper foil using a notch-bar, and by evaporating the solvent with a thermal treatment at 65 °C for 12 h under dynamic vacuum. The electrode sheets were pressed with a flat-plate press at ~7000 kPa, then transferred in an Ar filled glove-box (<0.1 ppm O_2 and H_2O), where they were punched in 7 mm diameter discs.

Na solid electrolyte was obtained by dissolving polyethylene oxide (PEO, Sigma Aldrich, average molecular mass 10^6) and sodium iodide (NaI, Sigma Aldrich, 99% purity) in acetonitrile (Sigma Aldrich, anhydrous, 99.8% purity). The relative amount between PEO and NaI was chosen so that the ratio between oxygen atoms in PEO chains and sodium atoms in NaI was 10:1. Aluminum oxide nanoparticles (Al_2O_3, Sigma Aldrich, average size of 13 nm, 99.8% purity) were added as a 10% of the total PEO + NaI mass, in order to improve Na-ion conductivity [53]. PEO, NaI, and Al_2O_3 were vacuum dried respectively at 50 °C for 20 h, at 300 °C for 12 h and at 300 °C for 24 h before use. The suspension was stirred for 12 h, then the solution was drop-cast on a Teflon base with cylindrical sockets and left at rest till the complete evaporation of the solvent. All processes were performed under Argon atmosphere (Schlenk glassware or Ar glove-box). After the drying process, 12 mm diameter electrolyte disks were obtained, with an average thickness of 0.3 mm. More details can be found in the Supplementary Information (SI).

Solid-state Na-ion half-cells were assembled using a stainless-steel split test cell (MTI Corporation, 20 mm inner diameter) sealed with silicone O-rings. Each half-cell was composed of the C_{60}- or $C_{60}H_x$-based electrode supported on the aluminum or copper collector and sodium metal (~1mm thickness, Sigma

Aldrich, 99.9% purity) as a counter electrode, separated by five plastic electrolyte disks. The temperature of the half-cell during measurements was kept at 60 °C, by using a previously calibrated Kapton heater (Minco Inc.) placed very close to the cell and powered by a DC power supply.

Powder X-ray diffraction (PXRD) measurements on discharged electrodes were performed either using a Bruker D8 Discover diffractometer operating in Debye-Scherrer geometry with an area detector (GADDS), or using a Bruker D2 Phaser diffractometer, operating in Bragg-Brentano geometry with a position sensitive detector (LYNXEYE), both equipped with a copper source (Cu Kα). In the former case, electrodes were detached from the collector and wrapped, then sealed in 0.7 mmm glass capillaries under Ar atmosphere. In the latter, the electrodes, still adherent to collectors, were placed in a suitable air-tight specimen dome with an O-ring, sealed under Ar atmosphere.

Cyclic voltammetry measurements (CV) were performed on the half-cells using a Keithley Sourcemeter 2400 at 0.01 V/s in the voltage range 0–3 V (vs Na/Na^+). The C_{60}- or $C_{60}H_y$-based electrodes were used as working electrodes, while metallic Na was used as counter and reference electrode, respectively. Galvanostatic charge/discharge measurements (GCD) were performed using a Kikusui DC Voltage/Current Standard Model 101 direct current source coupled with a Keithley Multimeter 2000 connected to a PC via RS-232. Typical acquisition time for the voltage and current values was every 1 s. Electrochemical impedance spectroscopy (EIS) measurements were performed with a HP 4192A impedance analyser in the frequency range 5 Hz–13 MHz, by applying a sine wave with amplitude of 0.1 V.

3. Results and discussion

3.1. Cyclic voltammetry

The first two redox cycles of the C_{60} electrode are shown in Fig. 1a. In the first sweep (in black), from 3 to 0.1 V (vs Na/Na^+), at least two reduction peaks are distinguishable, while during the second sweep, from 0.1 to 3 V, six oxidation peaks are well observed, respectively at 0.64, 0.91, 1.23, 1.49, 2.08 and 2.53 V vs Na/Na^+. During the second cycle (in blue), the peaks become even more evident, suggesting that the Na^+ electrochemical intercalation process in the cell is reversible under these conditions. All the observed peak potentials are reported in Table 1 and compared to previous cyclic voltammetry results obtained with C_{60} electrodes operating in different conditions, as reported vs the Na/Na^+ couple [31,33]. A very good correspondence, either in the peak potentials, or in peak separation between two successive reduction/oxidation, indicate that during Na^+ electrochemical intercalation all the six accessible redox C_{60} states were reached and up to 6 Na^+ ions per C_{60} molecule are reversibly inserted into the material. Further cycles show the same peak potentials observed at the second cycle, confirming that the intercalation process is reversible (see Figure S3).

The first two redox cycles of the $C_{60}H_x$ electrode are shown in Fig. 1b. The measurements confirm the stability of the hydrofullerite upon reduction. During the first cycle, only 3 peaks during the first sweep and 2 peaks during the second are detectable, while the second cycle shows 2 more peaks during the first sweep. A third cycle, showing the same peak potentials as the second one, confirming the reversible character of the processes, is displayed in Figure S4. Differently from the case of C_{60}, peak potentials appear not equally separated, as already observed for $C_{60}H_{36}$ [54]. All potential peaks are documented in Table 2.

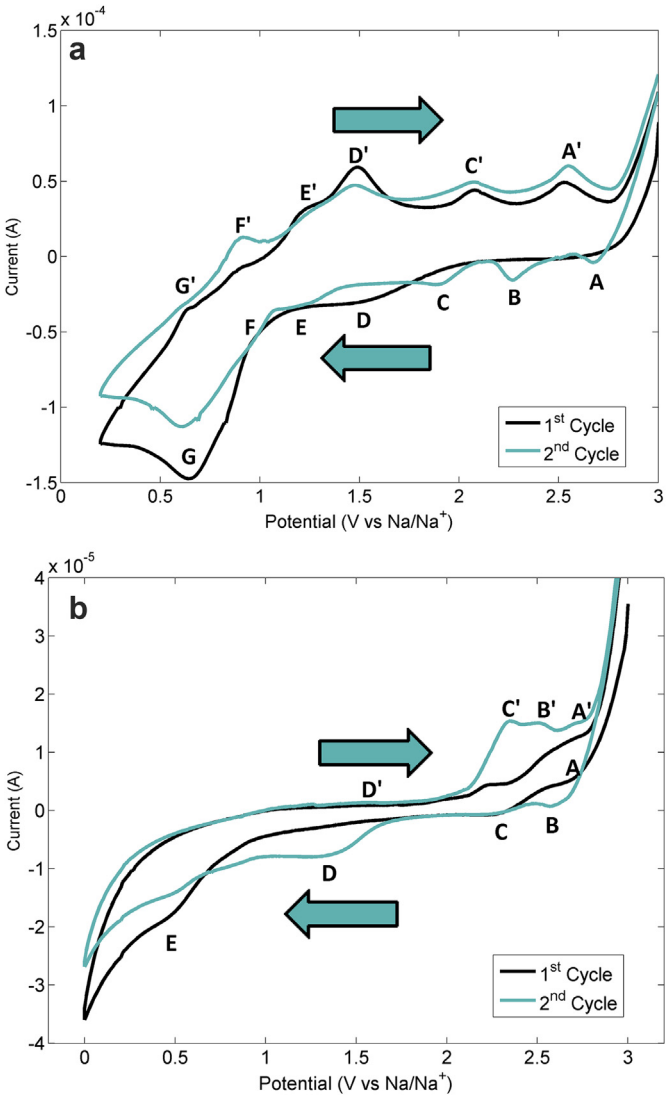

Fig. 1. CV of half cells with C_{60}-based electrode (a) and $C_{60}H_x$-based electrode (b). Starting potential is 3 V (vs Na/Na^+) and arrows indicate the sweep direction. The letters indicate the position of the oxidation/reduction peaks. (A colour version of this figure can be viewed online.)

3.2. Charge-discharge measurements

Solid-state half-cells made with C_{60}- and $C_{60}H_x$-based electrodes have been charged and discharged between their open circuit potential, 2.4 and 2 V (vs Na/Na^+) respectively, and 0.1 V at a fixed current of 1.5 μA, corresponding to a charge-discharge rate of 1/60 C. Both electrodes show large specific capacities during the first galvanostatic discharge (see Fig. 2a), respectively of 250 and 230 mAh/g. By integrating the current vs time we calculated the corresponding stoichiometry y in Na_yC_{60} and $Na_yC_{60}H_x$, which, at the complete discharge, turned out to be 6.8 and 6.5 respectively, assuming a homogeneous intercalation of the electrode materials.

Moreover, for both electrodes the first discharge potential is characterized by the presence of several plateaus, each marking a different electrochemical reaction process, whose corresponding potential and intercalation stoichiometry is reported in Table 3. It is worth noting that, for the C_{60}-based electrode, the observed plateau potentials match quite well those of the peaks E/E′, F/F′ and G/G′ observed in the CV curves, thus suggesting that the two

Table 1
CV Peak Potentials for C_{60} electrode.

Peak Index	1st Cycle Peak Potentials (V vs Na/Na^+)		2nd Cycle Peak Potential (V vs Na/Na^+)		Peak Potentials from Ref. [33] (V vs Na/Na^+)	Peak Potentials from Ref. [31] (V vs Na/Na^+)
	1st sweep	2nd sweep	1st sweep	2nd sweep		
A	–	–	2.68	–	-	–
A′	–	2.53	–	2.55	2.37	–
B	–	–	2.27	–	–	–
C/C′	–	2.08	1.90	2.07	1.98	2.0
D/D′	1.50	1.49	–	1.48	1.48	1.6
E/E′	–	1.23	1.21	1.30	-	1.2
F/F′	–	0.91	0.94	0.92	1.00	–
G/G′	0.65	0.64	0.61	–	0.50	0.5

Table 2
CV Peak Potentials for $C_{60}H_x$ electrode.

Peak Index	First Cycle Peak Potentials (V vs Na/Na^+)		Second Cycle Peak Potentials (V vs Na/Na^+)	
	1st sweep	2nd sweep	1st sweep	2nd sweep
A/A′	2.70	2.70	–	2.71
B/B′	-	–	2.58	2.51
C/C′	2.30	2.22	2.30	2.35
D	–	–	1.35	–
D′	–	–	–	1.56
E	0.47	–	0.49	–

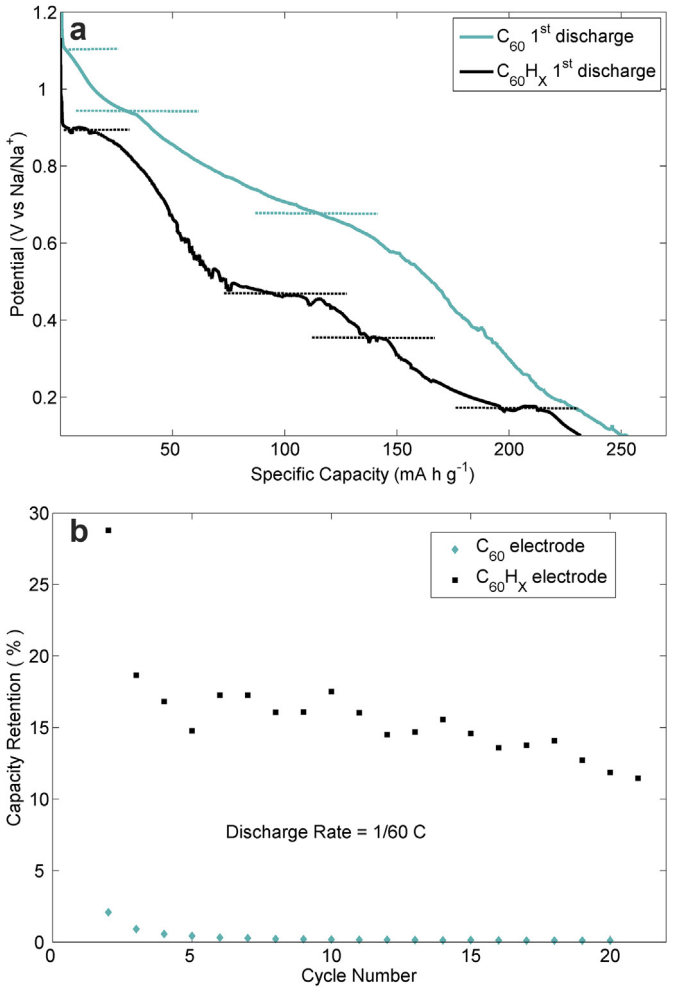

Fig. 2. Comparison of first discharge specific capacity of C_{60} and $C_{60}H_X$ half-cells (a) and comparison of capacity retention after the first cycle of C_{60} and $C_{60}H_X$ half cells (b). (A colour version of this figure can be viewed online.)

Table 3
Galvanostatic First Discharge Potential Plateaus and Stoichiometry (V vs Na/Na^+).

C_{60}		$C_{60}H_x$	
Potential Plateau (V)	Stoichiometry	Potential Plateau (V)	Stoichiometry
1.10	$Na_{0.1}C_{60}$	0.89	$Na_{0.4}C_{60}H_x$
0.93	$Na_{0.9}C_{60}$	0.46	$Na_3C_{60}H_x$
0.65	$Na_{3.5}C_{60}$	0.35	$Na_{4.1}C_{60}H_x$
End of discharge	$Na_{6.8}C_{60}$	0.16	$Na_{6.1}C_{60}H_x$
-	–	End of discharge	$Na_{6.5}C_{60}H_x$

techniques are probing the same electrochemical reactions. On the other hand, not all the reactions observed during the CV give rise to an evident plateau in the galvanostatic discharge, possibly indicating that some redox states of C_{60} do not have a counterpart in bulk Na^+ intercalation.

On the contrary, only the 0.5 V plateau in the $C_{60}H_x$ electrode confronts to a CV peak (E), while there is no clear connection between the other two observed plateaus.

The capacity retention of C_{60} and $C_{60}H_x$-based solid-state Na half-cells as a function of the charge/discharge cycles is shown in Fig. 2b. The C_{60}-based electrode presents a strong irreversibility of the specific capacity, which causes the half-cell to retain less than 1% of the initial capacity after few cycles. On the contrary, the $C_{60}H_x$-based electrode shows better reversibility, displaying a specific capacity of still 34 and 23 $mAhg^{-1}$, respectively at the 10th and 20th cycle. Although we expect that a significant fraction of the specific capacity observed during the first discharge could be due to the formation of SEI [55], the strong irreversibility found in the C_{60} electrode suggests that further irreversible processes should occur in this material upon Na^+ intercalation.

3.3. Powder X-ray diffraction

In order to better understand the different behavior probed during GCD measurements, PXRD was performed on both C_{60}- and $C_{60}H_x$-based electrodes in their discharged state (sodium inserted). Powder pattern for C_{60}-based electrode is shown in Fig. 3. The presence of many reflections in the 2θ range 8–37° reveals the formation of several crystalline phases; the majority of them can be easily ascribed to some already known Na_xC_{60} phases, in particular the cubic *fcc* phases, corresponding to $x = 2$ and $x \geq 6$ respectively [37], and the monoclinic polymeric phase corresponding to $x = 4$ [26]. The remaining broad peaks can be ascribed to PEO (at $2\theta = 19.2°$ and 23.2°). No reflections ascribable to metallic Na were detected.

The formation of different Na_xC_{60} phases witnesses the inhomogeneous Na^+ distribution of the bulk active material upon electrochemical intercalation, likely due to the presence of mechanisms hampering the Na^+ diffusion in the C_{60} electrode. A possible

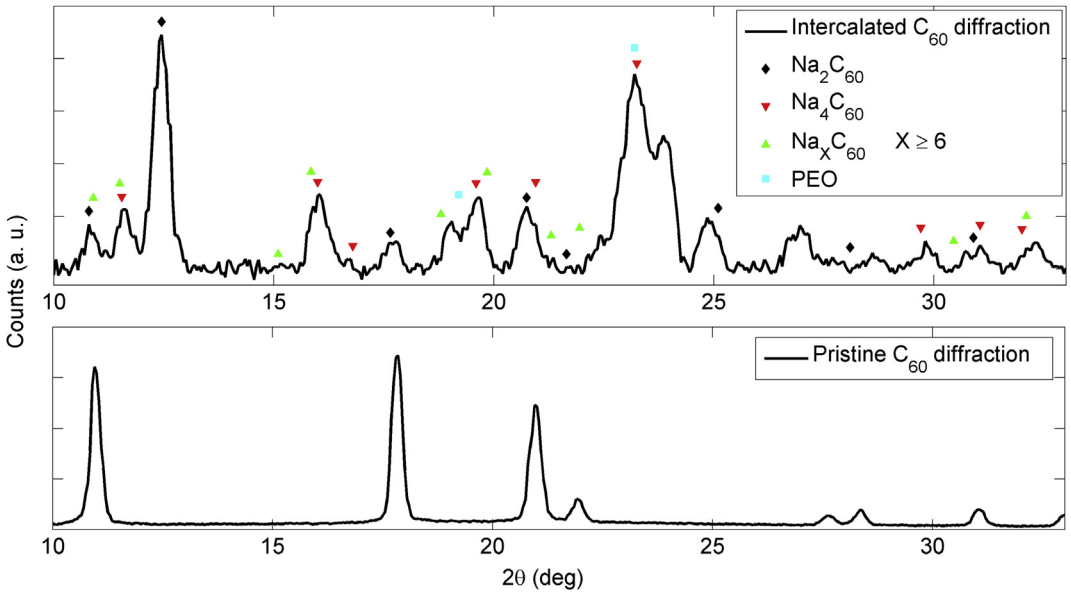

Fig. 3. PXRD pattern for the discharged C_{60} electrode (sodium inserted) and for the pure C_{60}. Peaks positions for different known sodium fullerides and for PEO are shown. (A colour version of this figure can be viewed online.)

explanation of this fact could arise from the different activation energies characterizing the Na^+ ion diffusion process in the different Na_xC_{60} crystal structures. In fact, alkali ion diffusion in the C_{60} network is a consequence of the metal ion hopping between neighboring accessible lattice interstices, which, in *fcc* C_{60}, consist of both tetrahedral and octahedral voids, generated by almost spherical fullerene packing. Such interstices are interconnected by trigonal apertures, whose size depends on the crystalline cell dimensions and symmetry, which can clearly change as a consequence of alkali intercalation. In particular, in the case of Na_xC_{60} phases, some evidences of inter-site diffusion of Na^+ ions were reported in monomeric *fcc* Na_2C_{60} and Na_6C_{60} phases, although at relatively high temperature (>400 K) [47,56,57]. On the contrary, no clear proofs of Na^+ diffusion exist for the Na_4C_{60} polymeric compound, probably because the polymerized C_{60} two-dimensional network hampers the inter-site mobility of Na^+ ion in this phase [48].

The concomitant formation of this phase in the C_{60} electrode could hence justify the observed irreversibility during the electrochemical intercalation.

Fig. 4 shows the diffraction pattern for a fully discharged $C_{60}H_x$ electrode. Unlike C_{60} electrode, in this case a low number of reflections were observed, which were tentatively indexed with a tetragonal cell ($a = b = 18.59$ Å, $c = 13.72$ Å, $\alpha = \beta = \gamma = 90°$). The comparison of the experimental powder pattern with that calculated from the $C_{60}H_x$ structure suggests that the observed diffractogram is compatible with a homogeneous Na^+ intercalated $C_{60}H_x$ phase, although the low quality of data does not allow a more detailed structural investigation. The absence of multiple phases in the discharged $C_{60}H_x$ also suggests a better Na^+ diffusion among the $C_{60}H_x$ interstices and is in agreement with the better reversibility observed in $C_{60}H_x$ electrodes.

3.4. Impedance analysis

Diffusion of Na^+ ions has been investigated also by means of EIS. The Nyquist diagrams for both C_{60}- and $C_{60}H_x$-based half-cells are shown in Fig. 5. They both consist of a slightly distorted semi-cycle plus a tail, which can be fitted with the equivalent circuit model shown in Fig. 6. The model comprises the impedance of the SEI (C_{SEI} and R_{SEI}), the impedance generated by the Na^+ ions diffusing between the electrode and the electrolyte (C_{CT} and R_{CT}) and the contribution due to the carrier diffusion through the electrode (C_{diff} and R_{diff}). R_0 and L are the contact resistance and the inductive effects due to the geometry of the battery, respectively. Fit parameters can be found in the SI (Table S1). In particular, we obtained $\rho_{diff} = 7.45$ MΩ cm for C_{60}-based electrode and $\rho_{diff} = 617$ kΩ cm for $C_{60}H_x$-based electrode. The rather large value found for the C_{60} electrode confirms its overall irreversible character towards Na^+ intercalation. On the other hand, $C_{60}H_x$ electrodes show clearly better performances in terms of Na^+ ion diffusion, which is in agreement with the previous results. The different fit values of SEI resistances for C_{60} and $C_{60}H_x$, of 1660 Ω and 730 Ω respectively (see Table S1), suggest the formation of a thicker SEI layer in the former, which could due to non-negligible solubility of C_{60}^{n-} in PEO [58].

4. Discussion

The observation of different crystalline Na_xC_{60} phases, with $x = 2$, 4 and 6, in the fully discharged C_{60}-based electrode, as shown by PXRD analysis, suggests that the observed irreversibility towards Na^+ bulk insertion, evidenced by GCD measurements, should be probably due to the formation of stable Na-intercalated fullerene compounds, in which Na^+ diffusion is prevented. In particular, C_{60} polymerization occurring in the Na_4C_{60} phase is expected to limit the apertures interconnecting the neighboring interstitial sites occupied by the intercalated Na^+ ion, thus blocking the inter-site Na^+ ion hopping process. In the case of $C_{60}H_x$ electrodes, PXRD analysis of the fully discharged anode is compatible with a more homogenous Na^+ distribution in the material. This suggests that either the increased steric hindrance of the hydrofullerenes, or their inability to form polymeric phases, due to the more saturated nature of the $C_{60}H_x$ molecule, could concur to increase the Na-ion diffusion in the hydrofullerene-based anode material. The EIS analysis carried out on these materials substantially confirmed this scenario.

The partial irreversible character affecting also $C_{60}H_x$ electrodes

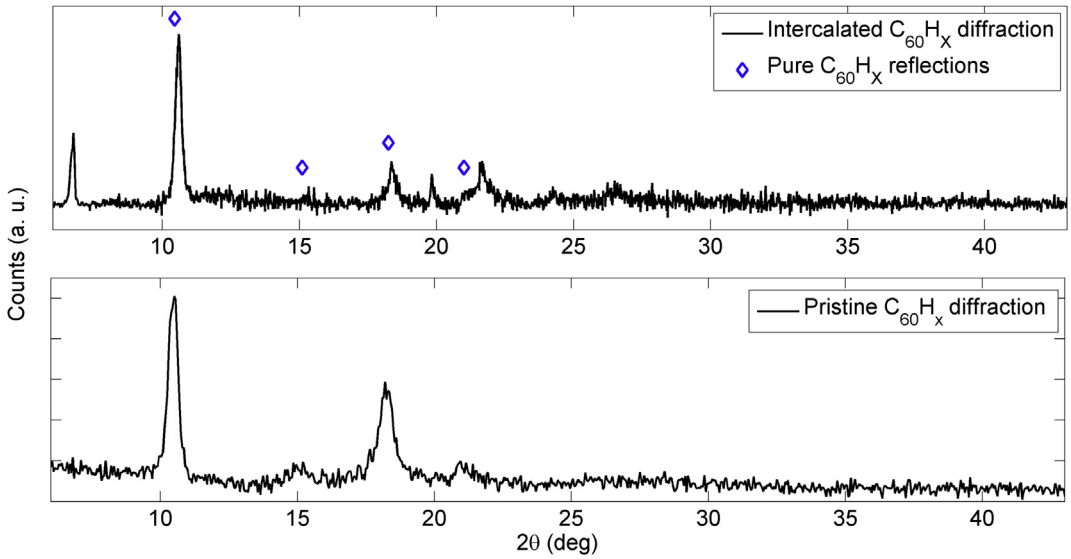

Fig. 4. PXRD pattern for the discharged $C_{60}H_x$ electrode (sodium inserted) and for the pure $C_{60}H_X$. No reflections corresponding to NaH or C_{60} can be observed. (A colour version of this figure can be viewed online.)

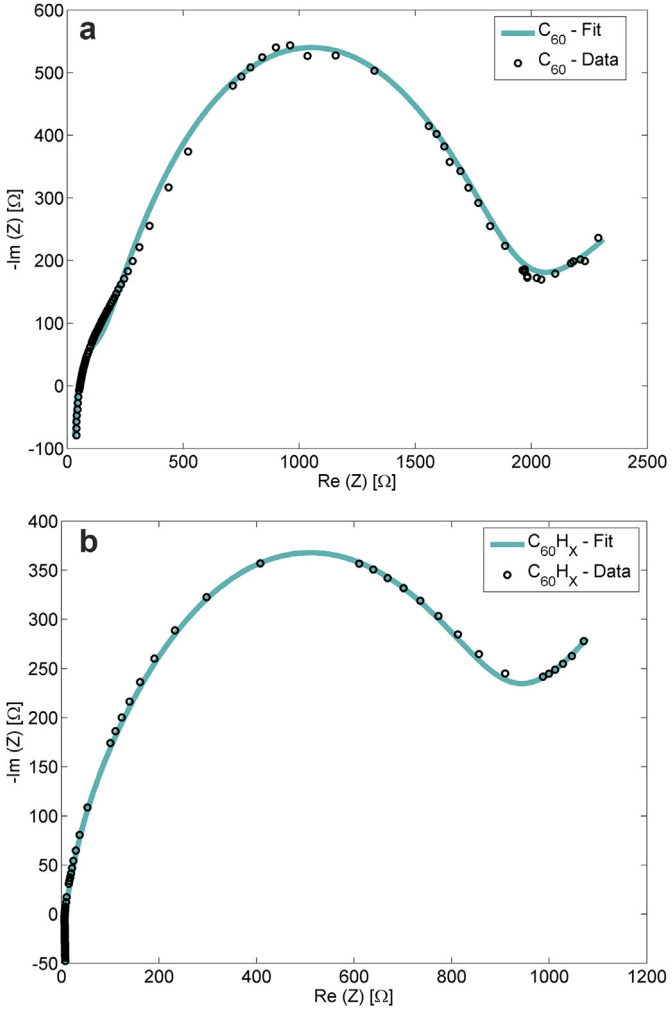

Fig. 5. Nyquist plot for EIS measurements on a C_{60}-based half-cell (a) and on a $C_{60}H_X$-based half-cell (b). (A colour version of this figure can be viewed online.)

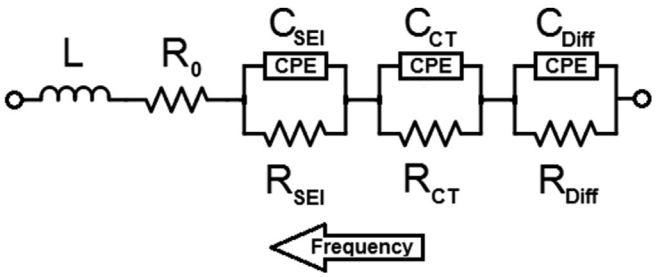

Fig. 6. Equivalent-circuit model for C_{60}-based and $C_{60}H_X$-based half-cells. L corresponds to inductive effects due to external factors and R_0 is the ohmic resistance of the battery. The model takes into account solid-electrolyte interphase (SEI) resistance at the Na metal surface (CSEI and RSEI), charge transfer occurring between $C_{60}/C_{60}H_X$ electrode and electrolyte (CCT, RCT), and carrier diffusion through the electrode (C_{Diff}, R_{Diff}).

could have several origins. One possibility could be the progressive contraction of the $C_{60}H_x$ lattice upon Na^+ intercalation, induced by the "chemical pressure" exerted by the charge transfer which is established between the small metal ions and the fullerene molecules [25,59]. This process is also expected to reduce the apertures interconnecting the intermolecular interstices, hence hampering the Na^+ ion diffusion inside the electrode. We exclude the formation of direct chemical reactions between H and Na, which would bring to the de-hydrogenation of the fullerene case, as no formation of NaH was observed from PXRD data on discharged electrodes (see Fig. 4). Other possible hydrogen-metal interactions, previously observed in hydrogen containing carbonaceous materials [60] are also excluded, due to the absence of sp^2 hydrogen terminated edges in the $C_{60}H_x$ molecule.

These results seems to go in the opposite direction with respect to those recently obtained in fullerene-based Mg-ion batteries [52]. In fact, the latter proved good reversibility performances, even at high-rate charge/discharge conditions, although the Mg^{2+} insertion is also expected to induce polymerization of C_{60} units. Similarly to what observed in Li fullerides, probably in this case the smaller ionic radius of Mg^{2+} ion, with respect to Na^+, plays a key role to allow the ionic diffusion even in a polymerized fullerene network.

5. Conclusions

The electrochemical insertion/extraction of sodium in C_{60}- and $C_{60}H_x$-based electrodes (with x~39) was studied through the preparation of solid-state Na-ion half-batteries, which were tested with CV, GCD measurements, PXRD and EIS. To this end, we developed a suitable Na solid-state electrolyte, in order to overcome the problem of the known solubility of C_{60} in common organic electrolytes used in batteries. CV performed on the half-cells confirmed the availability of up to six reversible red-ox states for C_{60}, accordingly to literature, and up to four reversible red-ox states for $C_{60}H_x$. The GCD measurements indicated that a significant amount of Na can be inserted in both C_{60}- and $C_{60}H_x$-based electrodes, which present a specific capacity of 250 mAh/g and 230 mAh/g at the first discharge respectively (corresponding to an average stoichiometry of $Na_{6\cdot8}C_{60}$ and $Na_{6\cdot5}C_{60}H_x$ respectively). However, the C_{60}-based electrodes displayed a strong irreversible behavior, which makes fullerene unsuitable as negative electrode material in secondary Na-ion batteries. Surprisingly, $C_{60}H_x$-based electrodes show significantly better performances upon cycling, in fact more than 10% of the initial capacity is retained after 20 cycles, even if, also in this case, results are still far from practical applications. The better reversibility of $C_{60}H_x$-based electrodes was ascribed to the increased steric hindrance of the hydrofullerenes, with respect to C_{60}, and to their inability to form polymeric phases, both factors which can increase the inter-site Na^+ diffusion upon cycling. Further studies of $C_{60}H_x$-based electrodes with different levels of hydrogenation are currently in progress, in order to evidence possible improvements of the results obtained so far.

Acknowledgements

The authors acknowledge C1P8 S.r.l. for the financial support, Solvay Specialty Polymers S.p.A. and TIMCAL SA-Group for reagents provisioning. M. Gaboardi acknowledges the European Union's Horizon 2020 research and innovation programme under the Marie Sklodowska-Curie Grant Agreement 665593 awarded to the Science and Technology Facilities Council.

Appendix A. Supplementary data

Supplementary data related to this article can be found at https://doi.org/10.1016/j.carbon.2017.12.107.

References

[1] M. Armand, J.M. Tarascon, Building better batteries, Nature 451 (2008) 652–657.
[2] J.M. Tarascon, M. Armand, Issues and challenges facing rechargeable lithium batteries, Nature 414 (2001) 359–367.
[3] M.D. Slater, D. Kim, E. Lee, C.S. Johnson, Sodium-ion batteries, Adv. Funct. Mater. 23 (2013) 947–958.
[4] V. Palomares, P. Serras, I. Villaluenga, K.B. Hueso, J. Carretero-Gonzalez, T. Rojo, Na-ion batteries, recent advances and present challenges to become low cost energy storage systems, Energy Environ. Sci. 5 (2012) 5884–5901.
[5] N. Yabuuchi, K. Kubota, M. Dahbi, S. Komaba, Research development on sodium-ion batteries, Chem. Rev. 114 (2014) 11636–11682.
[6] M.S. Dresselhaus, G. Dresselhaus, Intercalation compounds of graphite, Adv. Phys. 30 (1981) 139–326.
[7] P. Ge, M. Fouletier, Electrochemical intercalation of sodium in graphite, Solid State Ionics 28 (1988) 1172–1175.
[8] H. Kim, J. Hong, Y.-U. Park, J. Kim, I. Hwang, K. Kang, Sodium storage behavior in natural graphite using ether-based electrolyte systems, Adv. Funct. Mater. 25 (2015) 534–541.
[9] Y. Wen, K. He, Y. Zhu, F. Han, Y. Xu, I. Matsuda, Y. Ishii, J. Cumings, C. Wang, Expanded graphite as superior anode for sodium-ion batteries, Nat. Commun. 5 (2014) 4033.
[10] Q. Wang, C. Zhao, Y. Lu, Y. Li, Y. Zheng, Y. Qi, X. Rong, L. Jiang, X. Qi, Y. Shao, D. Pan, B. Li, Y.-S. Hu, L. Chen, Advanced nanostructured anode materials for sodium-ion batteries, Small 13 (2017) 1701835.
[11] M.-S. Balogun, Y. Luo, W. Qiu, P. Liu, Y. Tong, A review of carbon materials and their composites with alloy metals for sodium ion battery anodes, Carbon 98 (2016) 162–178.
[12] R. Alcántara, P. Lavela, G.F. Ortiz, J.L. Tirado, Carbon microspheres obtained from resorcinol-formaldehyde as high-capacity electrodes for sodium-ion batteries, Electrochem. Solid State Lett. 8 (2005) A222–A225.
[13] S. Komaba, T. Ishikawa, N. Yabuuchi, W. Murata, A. Ito, Y. Ohsawa, Fluorinated ethylene carbonate as electrolyte additive for rechargeable Na batteries, ACS Applied Materials & Interfaces 3 (2011) 4165–4168.
[14] A. Ponrouch, A.R. Goñi, M.R. Palacín, High capacity hard carbon anodes for sodium ion batteries in additive free electrolyte, Electrochem. Commun. 27 (2013) 85–88.
[15] Y. Cao, L. Xiao, M.L. Sushko, W. Wang, B. Schwenzer, J. Xiao, Z. Nie, L.V. Saraf, Z. Yang, J. Liu, Sodium ion insertion in hollow carbon nanowires for battery applications, Nano Lett. 12 (2012) 3783–3787.
[16] W.J. Li, S.L. Chou, J.Z. Wang, H.K. Liu, S.X. Dou, Simply mixed commercial red phosphorus and carbon nanotube composite with exceptionally reversible sodium-ion storage, Nano Lett. 13 (2013) 5480–5484.
[17] X. Zhou, Z. Dai, J. Bao, Y.-G. Guo, Wet milled synthesis of an Sb/MWCNT nanocomposite for improved sodium storage, J. Mater. Chem. 1 (2013) 13727–13731.
[18] Y.X. Wang, S.L. Chou, H.K. Liu, S.X. Dou, Reduced graphene oxide with superior cycling stability and rate capability for sodium storage, Carbon 57 (2013) 202–208.
[19] J. Xu, M. Wang, N.P. Wickramaratne, M. Jaroniec, S. Dou, L. Dai, High-performance sodium ion batteries based on a 3D anode from nitrogen-doped graphene foams, Adv. Mater. 27 (2015) 2042–2048.
[20] J.C. Pramudita, D. Pontiroli, G. Magnani, M. Gaboardi, M. Riccò, C. Milanese, H.E.A. Brand, N. Sharma, graphene and selected derivatives as negative electrodes in sodium- and lithium-ion batteries, ChemElectroChem 2 (2015) 600–610.
[21] J. Zhang, W. Lv, Y. Tao, Y.-B. He, D.-W. Wang, C.-H. You, B. Li, F. Kang, Q.-H. Yang, Ultrafast high-volumetric sodium storage of folded-graphene electrodes through surface-induced redox reactions, Energy Storage Materials 1 (2015) 112–118.
[22] J.C. Pramudita, A. Rawal, M. Choucair, D. Pontiroli, G. Magnani, M. Gaboardi, M. Riccò, N. Sharma, Mechanisms of sodium insertion/extraction on the surface of defective graphenes, ACS Applied Materials & Interfaces 9 (2017) 431–438.
[23] W. Krätschmer, K. Fostiropoulos, D.R. Huffman, The infrared and ultraviolet absorption spectra of laboratory-produced carbon dust: evidence for the presence of the C_{60} molecule, Chem. Phys. Lett. 170 (1990) 167–170.
[24] L. Forró, L. Mihály, Electronic properties of doped fullerenes, Rep. Prog. Phys. 64 (2001) 649.
[25] M. Riccò, T. Shiroka, M. Belli, D. Pontiroli, M. Pagliari, G. Ruani, D. Palles, S. Margadonna, M. Tomaselli, Unusual polymerization in the Li_4C_{60} fulleride, Phys. Rev. B 72 (2005) 155437.
[26] G. Oszlányi, G. Baumgartner, G. Faigel, L. Forró, Na_4C_{60}: an alkali intercalated two-dimensional polymer, Phys. Rev. Lett. 78 (1997) 4438–4441.
[27] D. Arčon, A. Zorko, M. Mazzani, M. Belli, D. Pontiroli, M. Riccò, S. Margadonna, The structural and electronic evolution of Li_4C_{60} through the polymer–monomer transformation, N. J. Phys. 10 (2008) 033021.
[28] A. Hebard, M. Rosseinsky, R. Haddon, D. Murphy, S. Glarum, T. Palstra, A. Ramirez, A. Kortan, Superconductivity at 18 K in potassium-doped C_{60}, Nature 350 (1991) 600–601.
[29] P. Wzietek, T. Mito, H. Alloul, D. Pontiroli, M. Aramini, M. Riccò, NMR study of the superconducting gap variation near the mott transition in Cs_3C_{60}, Phys. Rev. Lett. 112 (2014) 066401.
[30] C. Jehoulet, A.J. Bard, F. Wudl, Electrochemical reduction and oxidation of C_{60} films, J. Am. Chem. Soc. 113 (1991) 5456–5457.
[31] Y. Chabre, D. Djurado, M. Armand, W.R. Romanow, N. Coustel, J.P. McCauley, J.E. Fischer, A.B. Smith, Electrochemical intercalation of lithium into solid fullerene C_{60}, J. Am. Chem. Soc. 114 (1992) 764–766.
[32] C. Jehoulet, Y.S. Obeng, Y.T. Kim, F. Zhou, A.J. Bard, Electrochemistry and Langmuir trough studies of fullerene C_{60} and C_{70} films, J. Am. Chem. Soc. 114 (1992) 4237–4247.
[33] L. Echegoyen, L.E. Echegoyen, Electrochemistry of fullerenes and their derivatives, Accounts Chem. Res. 31 (1998) 593–601.
[34] R.O. Loutfy, S. Katagiri, Fullerene materials for lithium-ion battery applications, in: E. Ōsawa (Ed.), Perspectives of Fullerene Nanotechnology, Springer Netherlands, Dordrecht, 2002, pp. 357–367.
[35] S. Kawabe, T. Kawai, R. Sugimoto, E. Yagasaki, K. Yoshino, Electrochemical properties of fullerene derivative polymers as electrode materials, Jpn. J. Appl. Phys. 36 (1997). L1055.
[36] S. Lemont, J. Ghanbaja, D. Billaud, Electrochemical intercalation of sodium ions into fullerene, Mater. Res. Bull. 29 (1994) 465–472.
[37] M.J. Rosseinsky, D.W. Murphy, R.M. Fleming, R. Tycko, A.P. Ramirez, G. Dabbagh, S.E. Barrett, Structural and electronic properties of sodium-intercalated C_{60}, Nature 356 (1992) 416–418.
[38] T. Yildirim, O. Zhou, J.E. Fischer, N. Bykovetz, R.A. Strongin, M.A. Cichy, A.B. Smith Iii, C.L. Lin, R. Jelinek, Intercalation of sodium heteroclusters into the C_{60} lattice, Nature 360 (1992) 568–571.
[39] J.A. Teprovich, M.S. Wellons, R. Lascola, S.-J. Hwang, P.A. Ward, R.N. Compton, R. Zidan, Synthesis and characterization of a lithium-doped fullerane (Li_x-C_{60}-H_y) for reversible hydrogen storage, Nano Lett. 12 (2012) 582–589.

[40] P. Mauron, A. Remhof, A. Bliersbach, A. Borgschulte, A. Züttel, D. Sheptyakov, M. Gaboardi, M. Choucair, D. Pontiroli, M. Aramini, A. Gorreri, M. Riccò, Reversible hydrogen absorption in sodium intercalated fullerenes, Int. J. Hydrogen Energy 37 (2012) 14307–14314.
[41] M. Aramini, C. Milanese, D. Pontiroli, M. Gaboardi, A. Girella, G. Bertoni, M. Riccò, Addition of transition metals to lithium intercalated fullerides enhances hydrogen storage properties, Int. J. Hydrogen Energy 39 (2014) 2124–2131.
[42] D. Pontiroli, D. D'Alessio, M. Gaboardi, G. Magnani, C. Milanese, S.G. Duyker, V.K. Peterson, N. Sharma, M. Ricco, Ammonia-storage in lithium intercalated fullerides, J. Mater. Chem. A 3 (2015) 21099–21105.
[43] M. Riccò, M. Belli, M. Mazzani, D. Pontiroli, D. Quintavalle, A. Jánossy, G. Csányi, Superionic conductivity in the Li_4C_{60} fulleride polymer, Phys. Rev. Lett. 102 (2009) 145901.
[44] S. Rols, D. Pontiroli, C. Cavallari, M. Gaboardi, M. Aramini, D. Richard, M.R. Johnson, J.M. Zanotti, E. Suard, M. Maccarini, M. Riccó, Structure and dynamics of the fullerene polymer Li_4C_{60} studied with neutron scattering, Phys. Rev. B 92 (2015) 014305.
[45] L. Maidich, D. Pontiroli, M. Gaboardi, S. Lenti, G. Magnani, G. Riva, P. Carretta, C. Milanese, A. Marini, M. Riccò, S. Sanna, Investigation of Li and H dynamics in Li_6C_{60} and $Li_6C_{60}H_y$, Carbon 96 (2016) 276–284.
[46] N. Sarzi Amadè, M. Gaboardi, G. Magnani, M. Riccò, D. Pontiroli, C. Milanese, A. Girella, P. Carretta, S. Sanna, H and Li dynamics in $Li_{12}C_{60}$ and $Li_{12}C_{60}H_y$, Int. J. Hydrogen Energy 42 (2017) 22544–22550.
[47] N. Sarzi Amadè, D. Pontiroli, L. Maidich, M. Riccò, M. Gaboardi, G. Magnani, P. Carretta, S. Sanna, Molecular and ionic dynamics in $Na_xLi_{6-x}C_{60}$, J. Phys. Chem. C 121 (2017) 6554–6560.
[48] B. Sundqvist, O. Andersson, C. Gong, B. Liu, B. Tonpheng, J. Yu, M. Yao, AC impedance of A_4C_{60} fullerides under pressure, N. J. Phys. 17 (2015) 023010.
[49] D. Quintavalle, B.G. Márkus, A. Jánossy, F. Simon, G. Klupp, M.A. Győri, K. Kamarás, G. Magnani, D. Pontiroli, M. Riccò, Electronic and ionic conductivities in superionic Li_4C_{60}, Phys. Rev. B 93 (2016) 205103.
[50] A.S. Cattaneo, V. Dall'Asta, D. Pontiroli, M. Riccò, G. Magnani, C. Milanese, C. Tealdi, E. Quartarone, P. Mustarelli, Tailoring ionic-electronic transport in PEO-Li_4C_{60}: towards a new class of all solid-state mixed conductors, Carbon 100 (2016) 196–200.
[51] D. Pontiroli, M. Aramini, M. Gaboardi, M. Mazzani, A. Gorreri, M. Riccò, I. Margiolaki, D. Sheptyakov, Ionic conductivity in the Mg intercalated fullerene polymer Mg_2C_{60}, Carbon 51 (2013) 143–147.
[52] R. Zhang, F. Mizuno, C. Ling, Fullerenes: non-transition metal clusters as rechargeable magnesium battery cathodes, Chem. Commun. 51 (2015) 1108–1111.
[53] F. Croce, G.B. Appetecchi, L. Persi, B. Scrosati, Nanocomposite polymer electrolytes for lithium batteries, Nature 394 (1998) 456–458.
[54] A.S. Lobach, V.V. Strelets, Electrochemical behavior and parameters of hydrofullerene $C_{60}H_{36}$, Russ. Chem. Bull. 48 (1999) 2060–2064.
[55] S.J. An, J. Li, C. Daniel, D. Mohanty, S. Nagpure, D.L. Wood, The state of understanding of the lithium-ion-battery graphite solid electrolyte interphase (SEI) and its relationship to formation cycling, Carbon 105 (2016) 52–76.
[56] G. Klupp, P. Matus, D. Quintavalle, L.F. Kiss, É. Kováts, N.M. Nemes, K. Kamarás, S. Pekker, A. Jánossy, Phase segregation on the nanoscale in Na_2C_{60}, Phys. Rev. B 74 (2006) 195402.
[57] F. Rachdi, L. Hajji, M. Galtier, T. Yildirim, J.E. Fischer, C. Goze, M. Mehring, ^{13}C and ^{23}Na NMR studies of Na_2C_{60} and Na_6C_{60} fullerides, Phys. Rev. B 56 (1997) 7831–7834.
[58] D. Baril, Y. Chabre, Electrochemical time of flight investigation of C_{60} dissolution/diffusion into a polymer electrolyte, Electrochem. Solid State Lett. 4 (2001) E21–E24.
[59] M. Gaboardi, C. Milanese, G. Magnani, A. Girella, D. Pontiroli, P. Cofrancesco, A. Marini, M. Ricco, Optimal hydrogen storage in sodium substituted lithium fullerides, Physical Chemistry Chemical Physics 19 (2017) 21980–21986.
[60] T. Zheng, J.S. Xue, J.R. Dahn, Lithium insertion in hydrogen-containing carbonaceous materials, Chem. Mater. 8 (1996) 389–393.